Supporting Information

Selective Facet Reactivity During Cation Exchange in Cadmium Sulfide Nanorods

Bryce Sadtler[1,2], Denis O. Demchenko[3], Haimei Zheng[1,2], Steven M. Hughes[1], Maxwell G. Merkle[1], Ulrich Dahmen[2], Lin-Wang Wang[3], A. Paul Alivisatos[1,2]*

[1] Department of Chemistry, University of California, Berkeley, CA 94720

[2] Materials Science Division, Lawrence Berkeley National Laboratory, CA 94720,

[3] Computational Research Division, Lawrence Berkeley National Laboratory, Berkeley, CA 94720

*Corresponding author: alivis@berkeley.edu

SUPPLEMENTAL METHODS

I. Materials. All chemicals were used as received without further purification. Cadmium oxide (CdO, 99.99%), tetrakis(acetonitrile)copper(I) hexafluorophosphate ($[MeCN]_4Cu(I)PF_6$), sulfur (99.998%), acetone (HPLC grade, 99.98%) and the following anhydrous solvents: toluene (99.8%), methanol (99.8%), isopropanol (99.5%), chloroform (99%), and hexanes (95%) were purchased from Aldrich. Hexadecylamine (HDA, 99%), octylamine (OA, 99%), and nonanoic acid (NA, 96%) were purchased from Fluka or Aldrich. Octadecylphosphonic acid (ODPA) and tetradecylphosphonic acid (TDPA) were purchased from Polycarbon Industries (PCI Synthesis, 9 Opportunity Way, Newburyport, MA 01950, 978-463-4853). Trioctylphosphine oxide (TOPO, 99%) was purchased from Acros Organics or Aldrich. Trioctylphosphine (TOP, 97%) and tributylphosphine (TBP, 99%) were purchased from Strem Chemicals. Trioctylphosphine sulfide (TOPS) and tributylphosphine sulfide (TBPS) were prepared by mixing either TOP or TBP and sulfur together in a 1:1 molar ratio inside an argon glove box followed by stirring the mixture at room temperature until the sulfur was fully dissolved (typically ~ 24 hours for TOPS and ~ 1 hour for TBPS).

II. CdS nanorod synthesis. Colloidal CdS nanorods were synthesized under air-free conditions using standard Schlenk line techniques. For each reaction, CdO and varying

amounts of ODPA, TDPA and TOPO or HDA were added to a 25 mL, 3-neck flask (see Supporting Information Table 1 below for amounts). The contents of each flask were evacuated at 120ºC for > 20 minutes to remove water, and then the flasks were heated to 320ºC under argon for 20 to 30 minutes to enable the complexation of cadmium ions with the alkylphosphonic acid ligands. The reaction flasks were cooled back to 120ºC and again evacuated for one hour to remove water produced by the cadmium complexation. After the second evacuation step, the flasks were again heated to 320ºC under argon, and 2 g of TOP was injected into each flask. Then TOPS or TBPS was injected, and the nanocrystals were grown ~315ºC for at least 50 minutes. Secondary aliquots of TOPS or TBPS mixed with TOP were injected slowly via a syringe pump for reactions 1 and 2 (see Supporting Information Table 2). After cooling, a nonpolar solvent (hexane or toluene) and a surfactant (NA or OA) were added to the reaction flasks, and the solutions were transferred to air-free vials. Centrifugation was used to separate the nanocrystals from the remaining cadmium-phosphonate complex and the excess surfactants used in the reaction. The nanorods were washed several times with a combination of a nonpolar solvent (hexane or toluene), a surfactant (OA or NA), and a polar solvent (chloroform, acetone, isopropanol, or methanol) (see Supporting Information Table 3). The surfactants NA and OA help to break up the excess cadmium-phosphonate complex, which can form a gel when the reaction is cooled to room temperature. After each centrifugation, the supernatant was removed, and the precipitated nanorods were redispersed in fresh solvents. The final washing step was done without the surfactants NA or OA. The presence of excess octylamine was found to inhibit cation exchange of the CdS nanorods, as it binds to Cu^{+} ions in solution. After the washing steps, the nanorods were dispersed in toluene and stored in an argon glove box. This procedure produces some branched structures (i.e., bipods, tripods, and tetrapods) along with the rods. However, the majority of branched structures are removed during the washing steps, as they do not flocculate as easily as the nanorods and thus tend to stay in the supernatant. The Supporting Information Tables 1-3 below detail the synthetic conditions for the three batches of CdS nanorods used during these studies. An XRD pattern of the CdS nanorods produced in reaction 1 is shown in Figure 1. A TEM image of the CdS nanorods produced in reaction 2 is shown in Figure 2a.

Supporting Information Table 1. Amounts of CdO and surfactants used for each CdS nanorod synthesis and evacuation times for flasks

Reaction #	CdO (mg)	TOPO (g)	TDPA (g)	ODPA (g)	HDA (g)	First evacuation time (min)	Second evacuation time (min)
1	206	2.75	0.44	0.56	-	30	60
2	209	2.75	0.45	0.61	-	20	60
3	205	-	-	1.08	2.9	45	-

Supporting Information Table 2. Amount and time of sulfur precursor injections for each CdS nanorod synthesis

Reaction #	Total S:Cd molar ratio	Amount of 1st sulfur injection	Amount of 2nd injection	Secondary injection rate (mL/min)	Secondary injection start time (min)	Total reaction time (min)
1	4.3:1	1.3 g (TOPS)	1.5 g TOPS + 2.5 g TOP	0.05	25 min (after 1st injection)	~120
2	4.6:1	0.75 g (TBPS)	1 g TBPS + 1.55 g TOP	0.1	18 min (after 1st injection)	~65
3	2:1	1.3 g (TOPS)	-	-	-	~50

Supporting Information Table 3. Surfactants and solvents used to wash the CdS nanocrystals after synthesis

Reaction #	Solvents/ surfactants used for 1st washing step	2nd washing step	3rd washing step	4th washing step	5th washing step
1	toluene	toluene, OA	toluene, acetone	-	-
2	hexane, OA, acetone	toluene, OA, isopropanol	toluene, NA, isopropanol	toluene, isopropanol	toluene, isopropanol, methanol
3	toluene, OA, NA	toluene, OA, NA	toluene, chloroform	toluene, isopropanol	-

III. Cation exchange of CdS nanorods.

Supporting Information Table 4. Reaction conditions used to synthesize CdS-Cu_2S binary nanorods and Cu_2S nanorods by Cu^+ cation exchange of CdS nanorods

Cu_2S Sample #	CdS Reaction #	Cu^+/Cd^{2+}	$[Cu^+]$ (moles) in methanol (mL) and toluene (mL)	$[Cd^{2+}]$ in toluene	Method of mixing	TEM/XRD shown in Figure X
1	3	0.51	9.8×10^{-7} moles Cu^+ in 0.37 mL MeOH and 2 mL toluene	1.94×10^{-6} moles Cd^{2+} in 0.17 mL toluene	CdS soln. added to stirring Cu^+ soln.	4a
2	1	0.56	4.9×10^{-7} mol Cu^+ in 0.4mL MeOH + 1.8 mL toluene	8.8×10^{-7} mol Cd^{2+} in 0.28 mL toluene	CdS soln. added to stirring Cu^+ soln.	3, 4b
3	1	0.33	4.7×10^{-7} mol Cu^+ in 0.72 mL MeOH	1.4×10^{-6} mol Cd^{2+} in 3.1 mL toluene	Cu^+ soln injected via syringe pump at 0.015 mL/min to CdS solution	4c
4	1	0.6	4.4×10^{-6} mol Cu^+ in 0.8 mL MeOH + 5 mL toluene	7.3×10^{-6} mol Cd^{2+} in 0.425 mL toluene	CdS soln. added to stirring Cu^+ soln.	1
5	1	0.9	7.7×10^{-6} mol Cu^+ in 0.61 mL MeOH + 5 mL toluene	8.6×10^{-6} mol Cd^{2+} in 0.50 mL toluene	CdS soln. added to stirring Cu^+ soln.	1
6	1	1.2	1.0×10^{-5} mol Cu^+ in 0.81 mL MeOH + 5 mL toluene	8.6×10^{-6} mol Cd^{2+} in 0.50 mL toluene	CdS soln. added to stirring Cu^+ soln.	1
7	1	8.3	2.6×10^{-5} mol Cu^+ in 1.0 mL MeOH	3.1×10^{-6} mol Cd^{2+} in 3 mL toluene	Cu^+ soln. added to stirring CdS soln.	1
8	2	10	9.5×10^{-6} mol Cu^+ in 0.7 mL MeOH	9.5×10^{-7} mol Cd^{2+} in 2 mL toluene	Cu^+ soln. added to stirring CdS soln.	2b

IV. Inductively coupled plasma atomic emission spectroscopy. ICP-AES was used to determine the Cd^{2+} concentration for each CdS nanorod solution used in the cation exchange reactions. A Cd ICP/DCP standard solution (10,000 μg/mL Cd^{+2} in 2% HNO_3, Aldrich) was diluted into a series of Cd^{2+} concentrations spanning several orders of magnitude (50 ppb – 100 ppm). The acid concentrations were the same (1.2% nitric acid) in all of the standards. The area-integrated atomic emission lines (Cd: 228.8, 226.5, and 214.4 nm) were free from inter-element interferences and displayed a linear response over the entire concentration range measured. Samples were prepared such that the Cd concentration fell well within the linear dynamic range for at least one atomic line. The organic solvent was removed from each CdS nanorod solution by passing filtered (0.25 um pore-size) air over the nanocrystal solution. The remaining solids were then digested by adding a solution of concentrated nitric acid (69%, Ultra High Purity Trace Select by Fluka, Cd assay ≤ 0.00000005%). Three aliquots were measured for each sample, and the emission intensities were averaged over the three aliquots and the three emission lines. Typical molar extinction coefficients for Cd^{2+} within the CdS nanorod solutions were $3x10^6$ mol/cm^2 at 300 nm measured by visible absorption spectroscopy.

SUPPLEMENTAL MODELING

I. Relaxed Lattice parameters. The CdS, Cu_2S, and Ag_2S lattices used in our calculations of the interface formation energies were relaxed within the general gradient approximation (GGA) of density functional theory. The lattice parameters of the relaxed cells were used in all calculations and a comparison of these values to experimentally determined lattice constants are listed in Supporting Information Table 5 below. The lattice volumes, interaxial angles (α, β, and γ), and lattice parameter ratios (a/b and a/c) are the same for both the experimental and relaxed values.

Supporting Information Table 5. Comparison of experimental lattice parameters for CdS, Cu_2S and Ag_2S crystals to relaxed lattice parameters obtained within GGA

	Experimental parameters[1-3]						Relaxed parameters		
lattice	Space group	# formula units /cell	a (Å)	b (Å)	c (Å)	β (°)	a (Å)	b (Å)	c (Å)
CdS	P63mc (184)	2	4.1364	4.1364	6.7152	90	4.20	4.20	6.82
Cu_2S	P21/c (14)	48	15.246	11.884	13.494	116.35	15.350	11.965	13.586
Ag_2S	P21/c (14)	4	4.231	6.930	9.526	125.29	4.297	7.038	9.675

II. XRD simulations of the Cu_2S phase. $Cu_{2-x}S$ possesses several complex structures, which vary with both temperature and the Cu:S stoichiometry. The most common phases are the low temperature form of chalcocite ($x = 0$) and djurleite ($x = \sim 0.04$).[2,4,5] Both of these phases possess a slightly distorted, hexagonal closed-packed (hcp) sulfur sublattice, while the Cu atomic positions and stoichiometry are different for the two structures. The monoclinic unit cell of low chalcocite contains 48 Cu_2S formula units, while the djurleite unit cell has orthorhombic symmetry comprised of 1 $Cu_{189}S_{96}$ formula unit. X-ray diffraction patterns of fully converted Cu_2S nanorods were compared with simulated bulk powder diffraction patterns for different phases of Cu_2S, calculated using the Diamond program (http://www.crystalimpact.com/diamond/). The intensities and positions of diffraction peaks in the simulated pattern for low chalcocite match well with the experimental pattern of the fully converted nanorods (see Supporting Information Figure 1). Due to the significant overlap of diffraction peaks for CdS and Cu_2S, the patterns for the partially converted samples were not simulated. While the diffraction peaks apparent in the partially converted nanorods could potentially arise from Cu_2S as chalcocite in its low or high temperature forms or from djurleite, we assume that the Cu_2S material is in the low temperature chalcocite phase during all stages of the cation exchange reaction. The interfaces formed between low temperature chalcocite Cu_2S and the $(000\bar{1})$ and (0001) facets of wurtzite CdS have a low formation energy and different fractions of Cu_2S within the nanorods will have approximately the same amount of interfacial area with CdS. As the elastic strain energy should not change significantly for different segment lengths of Cu_2S, it is unlikely that a phase change occurs within the Cu_2S lattice as it grows within the nanorod.

III. Electron counting. For each interfacial S atom in the models of the CdS-Cu_2S epitaxial attachments, the optimal geometry should satisfy local electron counting rules, i.e. each S atom should have a local environment that supplies two electrons in order to fill the sulfur 3p bands. The orthorhombic Cu_2S lattice possesses a hexagonal sulfur sublattice, where for 24 S atoms in a layer, there are 16 intra-layer Cu atoms, and 32 inter-layer Cu atoms (16 interlayer Cu atoms on either side of the S layer). The supercell in Figure 5a shows orthorhombic Cu_2S connected to the $(000\bar{1})$ and (0001) end facets of CdS (I_1 and I_2, respectively), where the layers of Cu atoms are parallel to the interfaces. In I_1 the 24 S atoms at the interface each have three nearest Cd neighbors, and when 16 intra-layer and 16 inter-layer Cu atoms are removed to connect Cu_2S to CdS there are still 16 neighboring inter-layer Cu atoms. Counting electrons, each of the 24 S atoms is supplied with 1.5*e* per S atom from the 3 neighboring Cd atoms (0.5*e* per Cd nearest neighbor), while the 16 Cu atoms provide 16/24*e* per S atom. Each S atom would be fully coordinated if it were supplied with 2*e*, however at I_1 the coordination for each S atom is [2+(4/24)]*e*. Thus, removing 4 Cu atoms from I_1 satisfies electron counting for the interfacial sulfur layer. On the other hand, I_2 has 24 interfacial S atoms, each with one nearest Cd neighbor and 32 Cu atoms total (16 intra-layer and 16 inter-layer). Here the 24 S atoms are under-coordinated as each of the interfacial S atoms is supplied with 0.5*e* from the Cd nearest neighbor, and (16+16)/24*e* from the intra- and inter-layer Cu atoms. Each S atom in I_2 is supplied with [2-(4/24)]*e*, such that 4 more Cu atoms are needed at the interface to satisfy the electron counting. Thus, simply moving 4 Cu atoms

from I_1 to I_2 satisfies electron counting for both interfaces and preserves the Cu_2S stoichiometry. Unlike the end-on attachments, I_1 and I_2, described above, in the angled attachment of the monoclinic Cu_2S lattice to CdS (see Figure 5d), the layers of Cu atoms are at an angle of ~35° to the CdS-Cu_2S interface. In the side attachment of Cu_2S to CdS (see Figure 5e), the Cu layers are perpendicular to the interface. At these orientations were not able to satisfy electron counting for the interfacial S atoms in the supercell.

IV. Individual interface formation energies. In this section we show how to extract the individual formation energies, E_1^i and E_2^i, for the interfaces I_1 and I_2 shown in the CdS-Cu_2S supercell in Figure 5a. This supercell provides the average of the two energies, $(E_1^i + E_2^i)/2$. By computing the difference between the two energies, $E_1^i - E_2^i$, their individual values can be determined.

We first define the total energy of a CdS slab in a periodic geometry, infinite in the *xy*-plane, with two surfaces separated by vacuum along the *z* direction as:

$$E_{tot} = n_S\mu_S + n_{Cd}\mu_{Cd} + E^1_{surf} + E^2_{surf}, \qquad (1)$$

where, n_S and n_{Cd} are the numbers of sulfur and cadmium atoms, respectively, μ_S and μ_{Cd} are the corresponding chemical potentials, and E^1_{surf} and E^2_{surf} are the top and bottom surface energies of the CdS slab. We construct the supercells, shown in Figures 5b and 5c, which include a single CdS-Cu_2S interface and the opposite CdS and Cu_2S surfaces separated by vacuum. The supercell in Figure 5b contains the interface I_1 (connection of the (001) Cu_2S facet to the $(000\bar{1})$ CdS facet), along with a Cd-terminated (0001) CdS surface, and a $(00\bar{1})$ Cu_2S surface. The supercell in Figure 5c contains the interface I_2 (connection of the (001) Cu_2S facet to the (0001) CdS facet), along with a S-terminated $(000\bar{1})$ CdS surface, and the same $(00\bar{1})$ Cu_2S surface as in Figure 5b. The two CdS surfaces are passivated by pseudo-hydrogen atoms.[6] The Cu_2S surfaces were not passivated, however, tests showed that all the dangling bonds are localized on the surface, and there are no long-range electric fields. In order to cancel out the Cu_2S surface energies, both the supercells in Figures 5b and 5c connect the (001) facet of Cu_2S to CdS such that $(00\bar{1})$ Cu_2S surface is exposed for both supercells. Thus, the interface I_2 in Figure 5c is different from I_2 in Figure 5a, which connects the $(00\bar{1})$ facet of Cu_2S to CdS. However, as both I_2 connections to the (0001) CdS facet exhibit a similar bonding arrangement of interfacial Cu atoms, their formation energies should be similar. We also assume that the wurtzite, Cd-terminated (0001) CdS surface of the supercell in Figure 5b is equivalent to a zinc-blende, Cd-terminated (111) CdS surface. Likewise, we assume that the wurtzite, S-terminated $(000\bar{1})$ CdS surface of the supercell in Figure 5c is equivalent to a zinc-blende, S-terminated $(11\bar{1})$ CdS surface. Given that zinc-blende and wurtzite differ only in their stacking sequence of atomic layers parallel to these planes, this is a reasonable assumption. The total energies (per unit area containing one interfacial S atom) of these slabs can be expressed following the definition Eq. (1) as:

$$E_1 = E_{Cd}^{(111)} + \mu_{Cd} + E_1^i + n_{Cu}\mu_{Cu} + n_S\mu_S^{Cu_2S} + E_{surf}^{Cu_2S} + N(\mu_{Cd} + \mu_S^{CdS}) \qquad (2)$$

and

$$E_2 = E_S^{(11\text{–}1)} + E_2^i + n'_{Cu}\mu_{Cu} + n_S\mu_S^{Cu_2S} + E_{surf}^{Cu_2S} + N(\mu_{Cd} + \mu_S^{CdS}) \qquad (3).$$

Here, $E_{Cd}^{(111)}$ and $E_S^{(11\text{–}1)}$ are the (111)-type surface energies of Cd- and S-terminated zinc-blende CdS, respectively, E_1^i and E_2^i are the interface energies of I_1 or I_2, respectively, μ_{Cd}, μ_{Cu}, $\mu_S^{Cu_2S}$, and μ_S^{CdS} are the chemical potentials of atoms of Cd, Cu, S in the Cu_2S lattice, and S in the CdS lattice, respectively, $E_{surf}^{Cu_2S}$ is the energy of the unpassivated $(00\bar{1})$ Cu_2S surface, and N is the number of layers in the CdS slab. Note that Eq.(2) contains an extra μ_{Cd} term to account for the extra Cd layer in that structure. The last term in both Eqs.(2) and (3) is the energy of the bulk CdS lattice. Also, the atomic configurations of Cu_2S are not the same in the two structures, as indicated by different numbers of Cu atoms n_{Cu} and n'_{Cu}.

The difference between E_1^i and E_2^i can be computed if we eliminate all the unknowns in the Eqs.(2) and (3), such as the ill-defined individual chemical potentials in CdS and Cu_2S, and the surface energy terms. The surface energies $E_{Cd}^{(111)}$ and $E_S^{(11\text{–}1)}$ can be computed from wedge shaped cells of zinc-blende CdS following the recipe outlined by Zhang and Wei.[7] We construct CdS wedges shown in Supporting Information Figure 5a,b, which are passivated according to Ref. [4]. The first CdS wedge, in addition to the bulk contribution, contains two equivalent Cd-terminated (111) surfaces, one S-terminated (110) surface, and three corners. The second CdS wedge, in addition to the bulk contribution, contains two equivalent S-terminated $(11\bar{1})$ surfaces, one Cd-terminated (110) surface, and three corners. The corner contributions can be eliminated by taking the difference between the energies of two wedges of different sizes, where one has two more layers of CdS, and subtracting the chemical potential of the additional atoms (See Ref. [5] for a detailed derivation). Therefore, subtracting the bulk contributions of CdS and corner contributions, the surface energy of the wedge can be written as

$$E_3 = 2E_{Cd}^{(111)} + E_S^{(110)} \qquad (4)$$

or switching the S and Cd surface atoms (and passivants)

$$E_4 = 2E_S^{(11\text{–}1)} + E_{Cd}^{(110)} \qquad (5).$$

In turn, the (110) surface energies can be computed from the simple slab geometry shown in Supporting Information Figure 5c,d, and the corresponding surface energies can be written as

$$E_5 = 2E_{Cd}^{(110)} + \mu_{Cd} \qquad (6)$$

or switching the S and Cd surface atoms (and passivants)

$$E_6 = 2E_S^{(110)} + \mu_S \qquad (7).$$

Combining the equations (2)-(7) and taking into account that the interfaces are constructed in such a way that $n'_{Cu} - n_{Cu} = 1$, and $\mu_S + \mu_{Cd} = E_{CdS}^{bulk}$, and $\mu_S^{Cu_2S} + 2\mu_{Cu} = E_{Cu_2S}^{bulk}$, leads to the equation for the difference in formation energies for I_1 and I_2

$$E_1^i - E_2^i = (E_1 - E_2) - \tfrac{1}{2}\left[(E_3 - E_4) + \tfrac{1}{2}(E_5 - E_6)\right] - \tfrac{3}{4}E_{CdS}^{bulk} + \tfrac{1}{2}E_{Cu_2S}^{bulk} \qquad (8)$$

This construction allows us to compute individual formation energies of CdS-Cu_2S interfaces formed at the opposite ends of the rod, i.e. attaching Cu_2S to the wurtzite (0001) and (000$\bar{1}$) facets of CdS.

SUPPLEMENTAL REFERENCES

(1) Reeber, R. R.; Kulp, B. A. *Transactions of the Metallurgical Society of AIME* **1965**, *233*, 698-701.
(2) Evans, H. T. *Nature Physical Science* **1971**, *232*, 69-70.
(3) Sadanaga, R.; Sueno, S. *Mineralogical Journal* **1967**, *5*, 124-148.
(4) Morimoto, N. *Mineralogical Journal* **1962**, *3*, 338-344.
(5) Sands, T. D.; Washburn, J.; Gronsky, R. *physica status solida (a)* **1982**, *72*, 551-559.
(6) Wang, L.-W.; Li, J. *Physical Review B* **2004**, *69*, 153302-1-4.
(7) Zhang, S. B.; Wei, S.-H. *Physical Review Letters* **2004**, *92*, 086102-1-4.

.

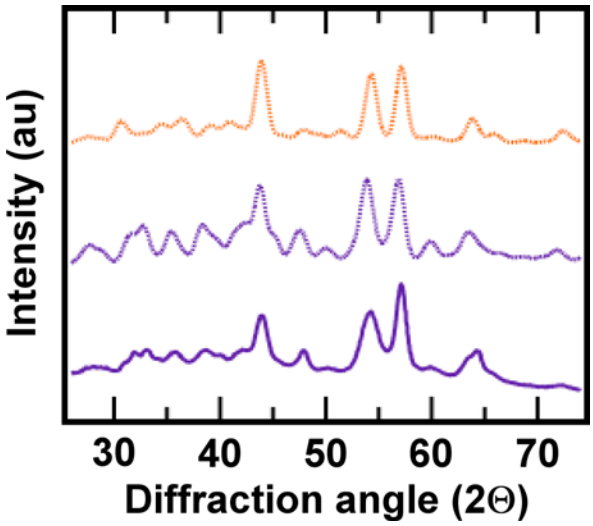

Supporting Information Figure 1. Experimental XRD pattern of Cu_2S nanorods made by cation exchange of CdS nanorods (bottom, purple) and simulated XRD patterns for bulk low-temperature chalcocite (middle, purple) and djurleite (top, orange). The peak positions and relative intensities of the experimental pattern for the Cu_2S nanorods match the simulated chalcocite pattern.

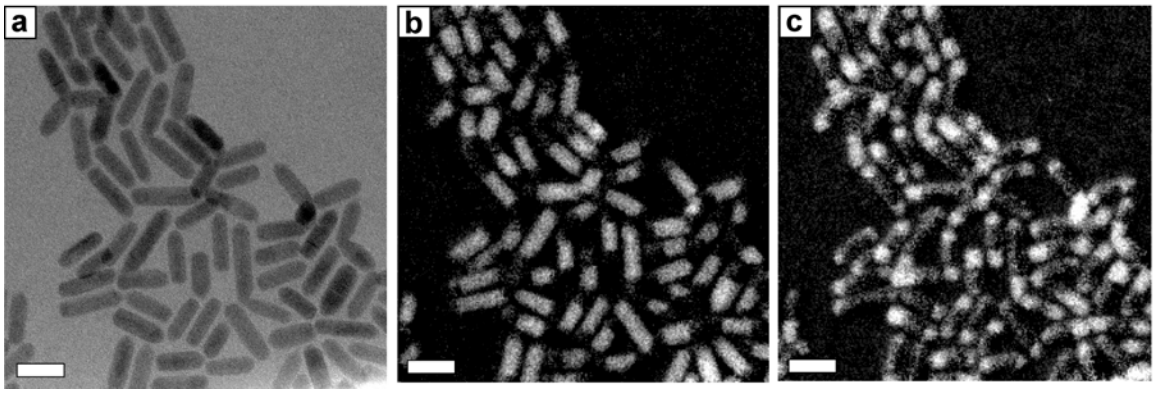

Supporting Information Figure 2. Original TEM images of the CdS-Cu_2S binary nanorods shown in Figure 3. (a) Bright-field (zero-loss) image. (b) Cd EFTEM image, (c) Cu EFTEM image. The lower energy of the Cu transition leads to a lower signal-to-noise for the Cu mapping. The scale bars are 20 nm for all 3 images.

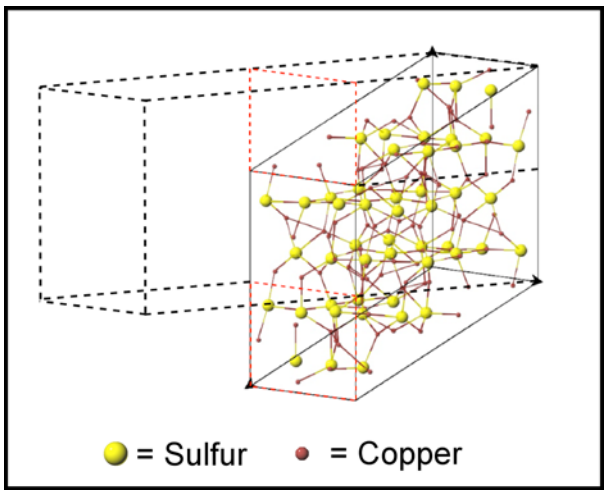

Supporting Information Figure 3. Relationship between the monoclinic unit cell of Cu_2S low temperature chalcocite and the pseudo-orthorhombic cell (outline) made by doubling the monoclinic cell.

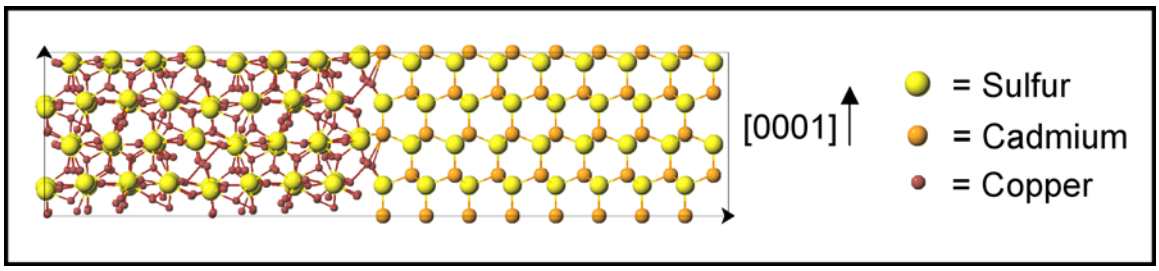

Supporting Information Figure 4. Supercell for the connection of Cu_2S to the $\pm(10\bar{1}0)$ side facets of CdS containing one unit cell of orthorhombic Cu_2S. The image shown in Figure 5e is the same interface but with the lattices extended along the CdS [0001] direction and shortened along the CdS $[10\bar{1}0]$ direction.

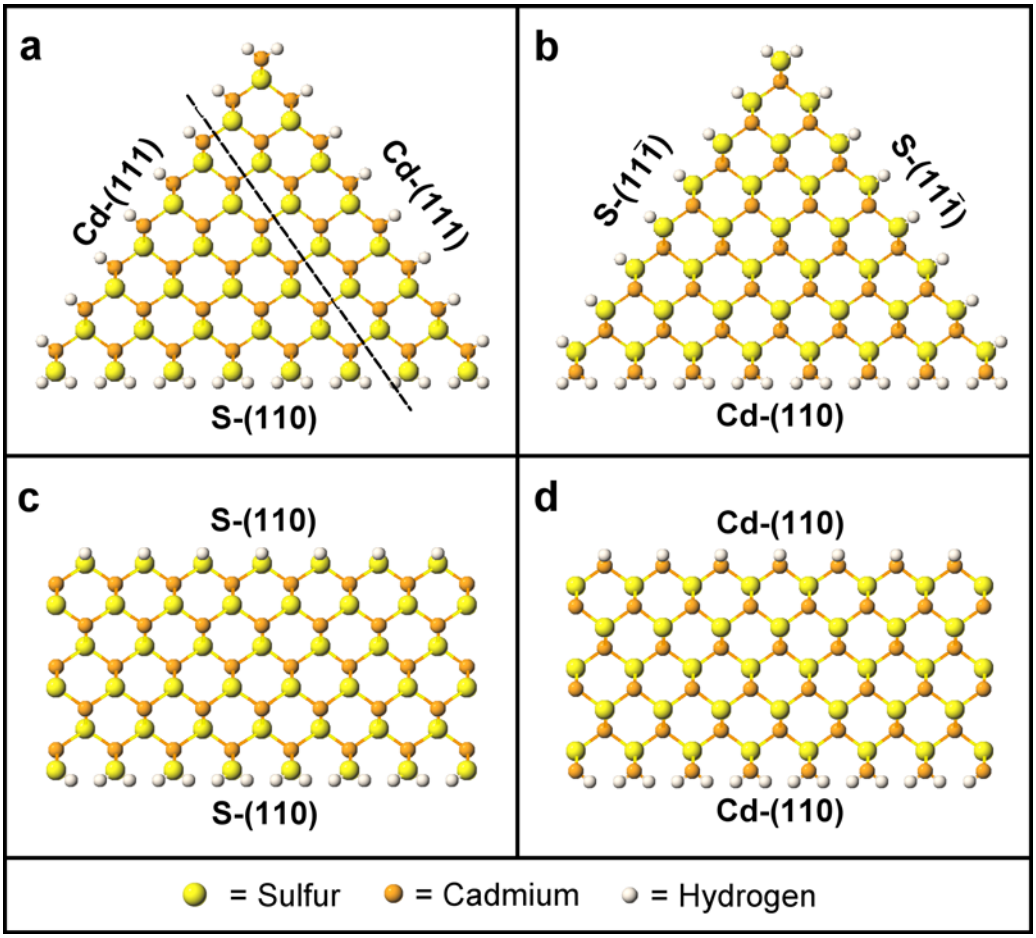

Supporting Information Figure 5. Auxiliary structures used to compute the surface energies of Cd- and S-terminated (111) and (110) facets of zinc-blende CdS. Each structure is infinite in the direction perpendicular to the page and the edges of each surface are labeled in the 2-D projections. (a) CdS wedge possessing two Cd-terminated (111) surfaces and one S-terminated (110) surface. (b) CdS wedge possessing two S-terminated (11$\bar{1}$) surfaces and one Cd-terminated (110) surface. The dashed line in (a) indicates wedges of different sizes used to remove the corner contributions from the surface energies. Slabs were used to subtract the (110) surface energies from each wedge. (c) CdS slab possessing two S-terminated (110) surfaces equivalent to that of the wedge in (a). (d) CdS slab possessing two Cd-terminated (110) surfaces equivalent to that of the wedge in (b).